International Symposium
On Turbulence and Shear Flow
Phenomena (TSFP-8)
August 28 - 30, 2013 Poitiers, France

NUMERICAL INVESTIGATION OF THE INFLUENCE OF UPSTREAM CONDITIONS ON PROPERTIES OF SHOCK NOISE IN SHOCK/MIXING LAYER INTERACTION

G. Daviller[†‡], G. Lehnasch[†1] & P. Jordan[†]
[†]Department of Fluid, Thermal and Combustion Sciences
Pprime Institute, CNRS-Université de Poitiers, ISAE-ENSMA
43 rue de l'Aérodrome, F-86036 Poitiers CEDEX, France
[‡]European Centre for Research and Advanced Training in Scientific Computation
31057 Toulouse, Cedex 1, France
[1]guillaume.lehnasch@isae-ensma.fr

ABSTRACT

A spatially developing two-dimensional mixing layer interacting with an incident compression wave is simulated in order to analyse the mechanisms leading to the shock noise emission. Various upstream forcing modes leading to various characteristics of subsequent travelling two-dimensional coherent structures are tested in order to assess their respective infuence on the leading mechanisms of shock leakage and subsequent shock noise properties.

INTRODUCTION

The pressure mismatch in slightly underexpanded jets leads to the formation of (diamond-shaped) shock-cells which strongly interact with the turbulent structures developing in the mixing layer around the potential core. This interaction process produces intense noise components on top of the turbulent mixing noise, which makes supersonic jets noiser than their subsonic counterpart (Tam (1995); Panda (1999)). In most cases, this intense sound production even drives a closed aeroacoustic loop by exciting the formation of instabilities in the upstream shear layer at the nozzle exit, leading to an intense tonal screech noise. Whereas the global phenomenology of this screech phenomena is now quite well understood, the physical process at the origin of the shock noise production itself remains to be clarified. It has been experimentaly observed for example by Panda (1999) that shock noise is mainly produced between the second and the fourth shock cell. This particular behaviour may be intuitively related to an appropriate strengh of interaction, thus combining a certain large-scale coherence characterizing the incoming turbulent eddies and an appropriate shock intensity. However, the precise local mechanisms which are here involved still need to be identified and quantified. A simplified flow configuration of an isolated shock reflecting on a mixing layer is a good surrogate flow configuration which may help in addressing this issue. Such a configuration has been retained for example by Manning (2000), Suzuki & Lele (2003), Lui & Lele (2003), Lui (2003) or Shaupp *et al.* (2008). By this way, a mechanism of shock leakage through vortex-ladden mixing layer was shown to play a fundamental role in shock noise emission. By means of geometrical acoustic theory, Suzuki & Lele (2003) also supported the idea that the local vorticity behaves as a barrier against shocks while acoustic waves can leak near the saddle point between vortices. The links between the local flow conditions and the exact properties of the sound emission yet remain unclear and the generality of such a mechanism remains to be explored to explain the shock noise properties in more complex situations. As a prerequesite to further analysis in complex three-dimensional full jets, a similar simplified approach is here followed to identify the physical mechanisms driving the intensity and directivity of shock noise as a function of inflow conditions. A two-dimensional interaction of a spatially developping mixing-layer with a compression wave is thus investigated by means of Direct Numerical Simulation (DNS) for a compression ratio of 1.2 and a transitional mixing layer, at a vorticity thickness based Reynolds number $Re_\omega = 2000$, separating a supersonic stream at $M = 1.2$ and a quiescent atmosphere.

NUMERICAL METHOD

The full compressible Navier-Stokes equations are here solved based on the non-dimensional formulation detailed in Shahab *et al.* (2011). In order to handle both shock/turbulence interaction and related acoustics, a high-order hybrid method has been implemented, switching from a skew-symmetric form of inviscid fluxes (Pirozzoli (2010)) discretized by an eighth-order accurate central differencing scheme in smooth regions to a seventh-order accurate WENO scheme (Shu & Osher (1988)) around shock discontinuities. A shock sensor based on the dilatation (Bogey *et al.* (2009)) is used to perform this switch. The viscous terms are discretized using classical eighth-order accurate central differencing scheme and the time marching is based on a fourth order Runge-Kutta algorithm. The computational domain and the treatment of boundaries are set up to fit the conditions used by Lui (2003) and are illustrated in figure 1.

The non-reflecting boundary conditions of Thompson (1987) are used in combination with damping sponges (Freund (1997)) around the computational domain, thus preventing any spurious reflections. Following the approach used by Freund (1997), a sixth-order low-pass filter is also

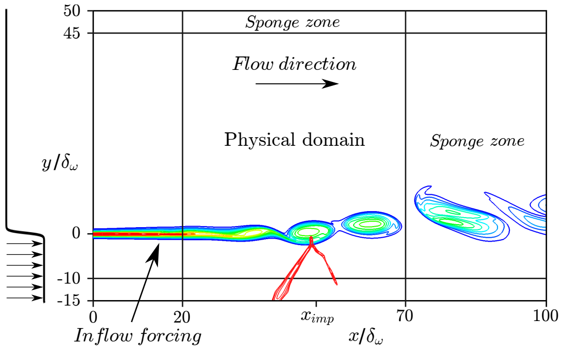

Figure 1. Computational domain and boundary treatment.

used along with the addition of a supersonic convection term (Ta'asan & Nark (1995)) and a grid stretching in the streamwise direction within the sponge region located just upstream of the domain exit. Finally, the conditions of incident compression/expansion waves are prescribed through the sponge region at the bottom of the computational domain. They are based on some classical two-dimensional inviscid relations (detailed for example in the work of Manning (2000)).

For the two-dimensional simulations, the domain is discretized by using 1920×650 points and extends within the range $0 \leq L_x/\delta_{\omega_0} \leq 100$ in the streamwise direction and $-15 \leq L_y/\delta_{\omega_0} \leq 53$ in the tranverse direction. The meshing procedure of Lui (2003) is here slightly modified in order to improve the refinement level in the streamwise direction within the interaction region and to increase the grid stretching in the transverse direction within the far-field top boundary. The physical portion of the domain extends from $20\delta_{\omega_0}$ up to $70\delta_{\omega_0}$ in the streamwise direction and from $-10\delta_{\omega_0}$ up to $50\delta_{\omega_0}$ in the tranverse direction. The mesh sizes in this region are $\Delta x = 0.025\delta_{\omega_0}$ and $\Delta y = 0.027\delta_{\omega_0}$ in the streamwise and transverse directions respectively. The mesh is then progressively stretched to reach $\Delta x(x/\delta_{\omega_0} = 0) = 0.6\delta_{\omega_0}$, $\Delta x(x/\delta_{\omega_0} = 100) = 1.15\delta_\omega$, $\Delta y(y/\delta_{\omega_0} = -15) = 0.15\delta_{\omega_0}$ and $\Delta y(y/\delta_{\omega_0} = 55) = 0.35\delta_{\omega_0}$ at the inlet, outlet, top and bottom boundaries respectively.

An error function is used to define the inflow profile and to initialize the mixing layer. The lower part of the shear layer is at Mach $M_1 = U_1/c_\infty = 1.2$, whereas the upper side is quiescent, with $U_2 = 0$. The flow Reynolds number, based on the inflow vorticity thickness and the velocity difference between the two streams is $Re_{\omega 0} = \delta_{\omega 0}\Delta U/\nu_\infty = 2000$. In addition, the transversal velocity is initially set to zero, pressure is kept constant and equal to the ambiant value, and the inflow temperature profile is determined by a Crocco-Busemann relation.

NUMERICAL REFERENCE CASES

Following Shaupp *et al.* (2008), a forcing procedure is used in order to promote the development of vortical structures within a reasonable distance. It is based on small perturbations of the velocity components following a random walk process acting on the individual phase at each forced frequency. For each case considered, after a numerical transient of around $t \simeq 600$, the database has been collected over 60 periods corresponding to $1/20f_o$, where f_o is the frequency of the most unstable mode for the hyperbolic tangente profile used at inlet.

Four cases of two-dimensional shock/mixing layer interactions have been considered in the present study. They differ by the selection of various subsets of these inflow perturbation modes, detailled in table 1. The other key parameters are kept constant, including the location for the interaction $x_{imp=} = 50\delta_\omega$, the width of the compression fan in the interaction region $w_{cw} = 2.5\delta_\omega$, and the overal compression level $\Delta p/p_\infty = 0.2$.

Case	N	f
A	1	f_o
B	1	$0.5f_o$
C	2	fo and $0.5f_o$
D	40	$0.5f_o \leq f \leq 2f_o$

Table 1. Inflow forcing parameters for the various simulation cases. N represents the number of forcing modes.

Both the reference Reynolds number and the spectral content of the inflow perturbation are likely to influence the overall features of the successive steps of the growth of the coherent structures (amplification rate, begining of rolling, level of coherence, delay before pairing, etc). In order to get the possibility to control as far as possible the various types of coherent events travelling through the interaction region, the upstream forcing had to be controlled carefully so that the growth of the various types of coherent events keep a comparable amplitude just upstream of the interaction. A maximal amplitude of the inflow perturbations equal to $\alpha = 0.007U_1$ was empirically found to be a good compromise for this purpose. For each case, the saturation of the intensity of fluctuating pressure, illustrated in figure 2, is thus obtained just upstream of the interaction region, whatever the origin or amplification rate is.

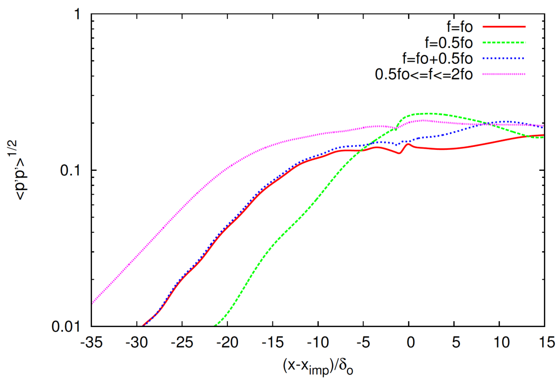

Figure 2. Streamwise evolution of the intensity of fluctuating pressure upstream of the interaction region (x_{imp} is the interaction position, δ_0 the initial vorticity thickness).

By this way, the interactions of the compression fan with various well identified privileged behaviors of the shear layer are considered: fundamental mode (case A), stronger eddies, more spaced (case B), forced upstream pairing at fixed frequency and position (case C) and natural random development (case D).

MEAN FLOW FEATURES

The influence of the various upstream conditions on the mean flow properties are first briefly examined in this section. For the sake of conciseness, only the mean and fluctuating pressure, and the shear turbulent shear stress are here reproduced for cases A and B in figures 3 and 4.

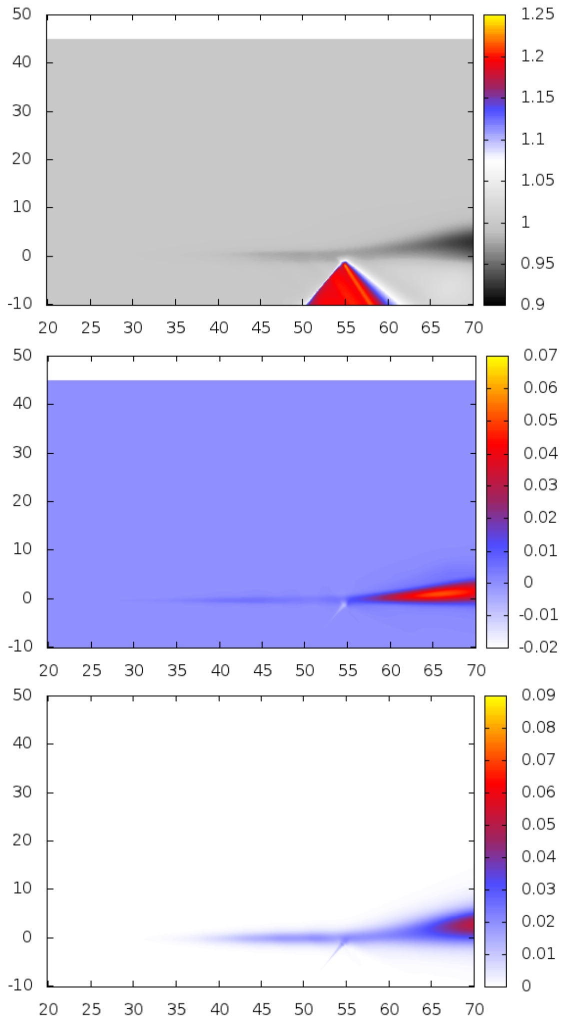

Figure 3. Mean flow properties of the interaction for simulation case A ; from top to bottom: $\overline{P/P_\infty}$, $\overline{u'v'/U_\infty^2}$, $\overline{p'^2/P_\infty^2}$.

For all cases, the same expected features are yet obviously observed, including the presence of the incoming compression fan reflecting into an expansion fan and the outward deflection of the shear layer downstream of the interaction zone. Some important differences are however highlighted. By comparison with the reference case A, the compression fan appears more diffused within the interaction zone when the subharmonic forcing mode is considered (case B or C). An overshoot of the prescribed compression rate is also noticed downstream of the compression fan in these cases. This seems to indicate a stronger mutual influence of the the compression fan and the intrinsic dynamic of the shear layer, associated with a larger excursion of the shock position. The peak of pressure variance and the sudden interuption of the growth of the shear zone, just downstream of the interaction point in these cases confirm this observation. For case D, the mean shear region (associated

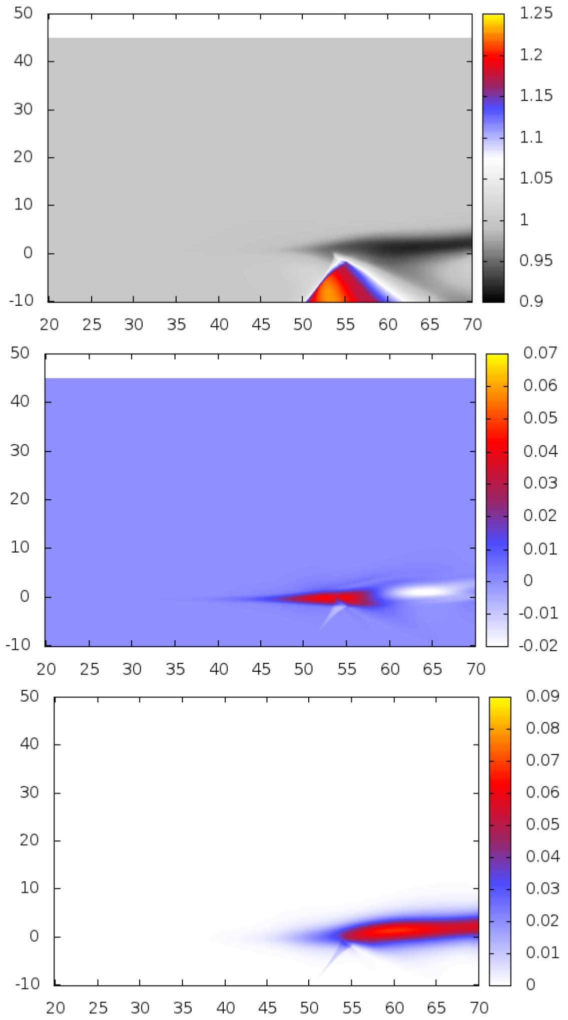

Figure 4. Mean flow properties of the interaction for simulation case B ; from top to bottom: $\overline{P/P_\infty}$, $\overline{u'v'/U_\infty^2}$, $\overline{p'^2/P_\infty^2}$.

with a significant decrease of the mean pressure) spreads in a more important way. This is consistent with the fact that the development of the shear layer is more natural in this case and yield random appearance and pairing of eddies travelling within a more extented region. We may legitimely consider that the potential acoustic energy of shock-noise could be related to both the effective local compression rate (thus to the difference between the mean pressure within the shear layer in the upstream zone and the imposed pressure level downstream of the compression fan) and to the intensity of fluctuations (related to the deformation rate of convected eddies). Accordingly, the present statistical characteristics already give some hints indicating for example that forcing with the subharmonic mode is likely to lead to a more intense shock-noise.

NOISE PROPERTIES

The instantaneous features of the interaction zone are first classically illustrated in figure 5 for case (A) by means of isocontours of vorticity superimposed to the field of divergence of velocity. These features are in good qualitative agreement with the visualizations of Lui & Lele (2003). This particular instant of the shock leakage cycle is observed during the passage of a convected eddy, ahead of the pending new shock noise sound emission. The deformation of the tail of the compression fan which focuses within the vortex can be noticed by the perturbation of the dilatation field in the lower part of the vortex, while the traces of four of the previous sound emissions associated to the previous passages of vortices are still observed in the surrounding quiescent atmosphere. The purple line here indicates the location of the arc of signal probes used to analyse the spectral properties of shock noise.

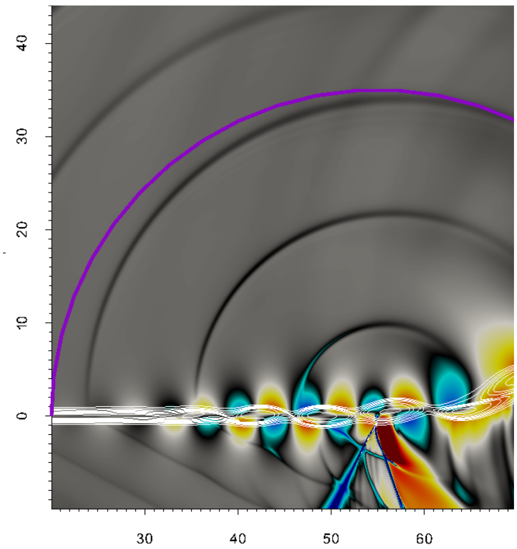

Figure 5. Shock leakage mechanism (case A), represented by an isosurface of the dilatation field (color) and contours of vorticity (white lines); arc of signal probes at $r = 35\delta_0$ from the interaction (purple).

The power spectral densities of pressure signals are illustrated in figure 6 for the various cases considered and for angles varying in counterclockwise direction. The black vertical lines indicate the forced mode(s) or range of modes used for triggering the mixing layer development. From a global point of view, the energy levels of pressure fluctuation are found to increase in the downstream direction. This observation is consistent with the fact that the signals are still acquired in a zone where the hydrodynamic fluctuations dominate, with a prefered noise radiation in the downstream direction. The peaks of energy levels at the forced frequencies are however quite similar whatever the position of the probe considered. This indicates that the shock-noise emission remains mainly omnidirectional. Interestingly, the use of only the subharmonic forcing mode (case B) significantly dampens the contributions of highest frequencies in the downstream direction whereas they are enhanced when both dominant and subharmonic modes are used together. For case D, the more natural development of the shear layer naturally leads to the disappearance of the energy peaks.

Due to the proximity to the hydrodynamic zone, the respective contributions of the shock noise and the turbulent noise are ambiguous. Following the approach of Suzuki & Lele (2003), the construction of a directivity plot may be attempted by filtering the low frequency range, assuming that this range mainly corresponds to the hydrodynamic field. The evolution of the resulting signal power is reproduced for example in figure 7 for case A for which the filtered

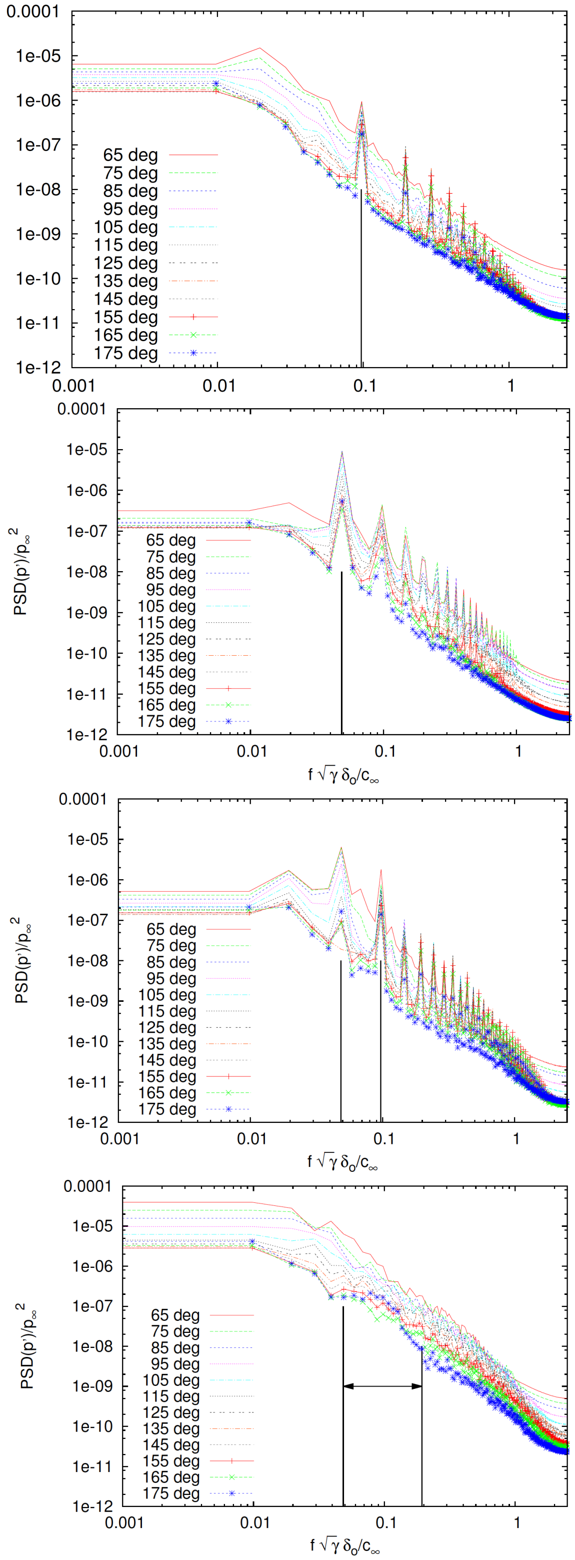

Figure 6. Power spectral distributions of pressure fluctuations at probes located at $r = 35\delta_0$ from the interaction region (see figure 5.

range extends up to three times the dominant forcing frequency. The trend (prefered upstream propagation of shock noise) predicted by these authors by means of geometrical theory is thus recovered, but with a large discrepency in the amplitude. It is found in fact that this amplitude significantly varies as a function of the exact spectral window used for carrying out this filtering process. In addition, we should recall that the forcing methods are not similar in both studies, which could explain some differences in the exact levels of coherence of travelling structures and thus strength of interaction with the shock, leading to different amplitudes of shock noise. Such a different upstream rate of amplification of vorticity can also alternatively be obtained by varying the reference Reynolds number. The resulting directivity plot is added in figure 7 (for a Reynolds number equal to 500 instead of 2000) to illustrate this dependance of the shock-noise to the intensity of upstream coherent structures travelling through the interaction region.

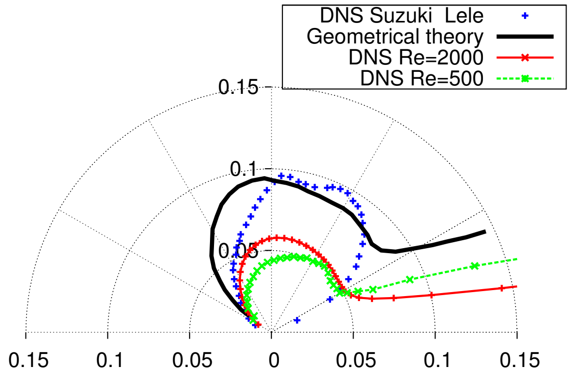

Figure 7. Directivity plots of filtered pressure wave amplitude issued from the interaction region (case B).

SHOCK-LEAKAGE PHENOMENON

The various elements given in the previous sections illustrate the difficulty to interpret properly the shock noise, based only on statistical information. From an instantaneous point of view, the replication of the more intense sound emission can yet clearly be associated to the end of every passage of convected eddies in agreement with the observations of Manning (2000) or Suzuki & Lele (2003). However, the phenomenological description of the emergence of the sound emission and the local flow properties which are likely to drive its intensity remain to be clarified.

In order to gain more insight in the local instantaneous mechanisms leading to the sound emission, some snapshots of the flowfield during a shock-leakage cycle (of period T) are thus examined and reproduced in figure 8. The visualization is based on the application of a combination of bilaplacian and gaussian filters to the divergence of the velocity field. Such filters are classicaly used to extract the contours of objects in image processing and enable in the present case to better contrast the presence of small-amplitude local waves within the interaction region, which would be masked by the levels of divergence naturally associated with the compressible incoming coherent structures.

At the first time instant illustrated $t^*/T = 0.0$, the fan expansion nearly focuses in the middle of the bottom part of the travelling eddy. At each instant, the small modifications of local conditions are associated with the emergence of acoustic perturbations which travel both in the downstream part of the supersonic flow and within the vortex. In this vortex, the direction of the front of acoustic waves

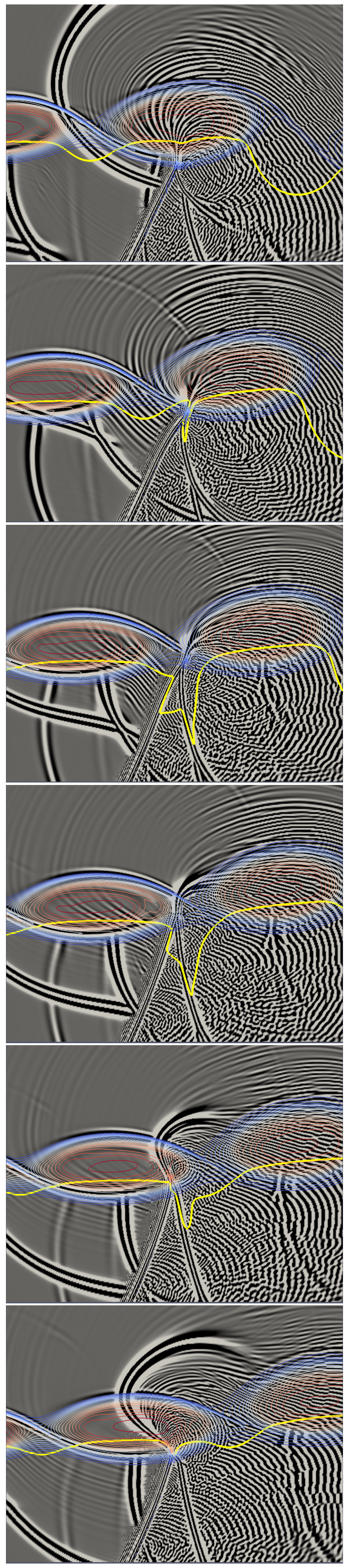

Figure 8. Shock-leakage phenomenon visualized with successive snapshots of isocontours of vorticity (color scale) and sonic line (yellow line) superimposed on (bi-laplacian) filtered field of divergence of velocity (grey scale): $t*/T = 0.0, 0.3, 0.46, 0.56, 0.66, 0.76$.

is progressively adapted as a function of the local curvature of streamlines, so that most of this acoustic perturbations appear to be contained within the coherent structure while a small part of energy escapes. Some interesting features are observed at the second time instant $t^*/T = 0.3$ which seems to correspond in fact to the true origin of the shock noise emission. At this step, the local distortion of the velocity field becomes sufficiently important that it leads to the appearance of a subsonic zone downstream of the shock while small waves have already begun to escape in the upstream direction above the braid separating the eddy from its following partner. The origin of shock noise is generally associated with the following time instant for which the compression fan targets the middle of the braid between the two successive eddies. However, at this second step, the shock tip already clearly appears to become a wave propagating towards the quiescent atmosphere. At the following time instant $t^*/T = 0.46$, this propagating wave yields two distinct parts. The first part is located underneath the braid and will propagate within the following travelling eddy. The second part, located above the vorticity braid, escapes within the atmosphere. The extension of the subsonic zone included in the supersonic stream reaches it maximal value at this step before decreasing while the portion of the front wave above the braid escapes. The flow topology then tends to come back to its original stage within the following vortex. These observations thus support the idea that the shock noise properties can not be related only to the distribution of vorticity. The exact orientation and extent of the compression fan and the subsequent extension of the subsonic region appearing underneath the braid region could possibly be also an essential ingredient.

SUMMARY

A two-dimensional mixing layer interaction with a compression wave has been simulated for various upstream conditions obtained by triggering various subsets of perturbation modes. The inflow conditions leading to the formation of the more intense and extended coherent strutures were found to lead both to the more important local increase of pressure fluctuations and to the maximal amplitude of the sound emission. Highly contrasted visualizations of the contours of the divergence field during the shock-leakage cycle have confirmed previous observations of the crucial role of the topology of coherent structures acting like a barrier against the focusing shock. They also confort the idea that more coherent structures, such as the one resulting from a pairing event forced by the use of subharmonic mode naturally leads to more elongated braids of vorticity, allowing locally more intense sound emissions. Some possible links between the shock-noise intensity and directivity with the formation and extension of the subsonic region growing locally underneath this braid region remains to be explored.

ACKNOWLEDGEMENTS

This work was granted access to the HPC resources of IDRIS and TGCC under the allocations x2012020912 and x20132a0912 made by GENCI (Grand Equipement National de Calcul Intensif).

REFERENCES

Bogey, C., de Cacqueray, N. & Bailly, C. 2009 A shock-capturing methodology based on adaptative spatial filtering for high-order non-linear computations. *J. Comp. Physics* **228**, 1447–1465.

Freund, J.B. 1997 Proposed inflow/outflow boundary condition for direct computation of aerodynamic sound. *AIAA Journal* **35** (4), 740–742.

Lui, C. C. M. 2003 A numerical investigation of shock-associated noise. PhD thesis, Stanford University.

Lui, C. C. M. & Lele, S. 2003 Sound generation mechanism of schok-associated noise. In *9th AIAA/CEAS Aeroacoustics Conference and Exhibit*, , vol. AIAA 2003-3315. Hilton Head, South California.

Manning, T. A. 2000 A numerical investigation of sound generation in supersonic jet screech. PhD thesis, Stanford University.

Panda, J. 1999 An experimental investigation of screech noise generation. *J. Fluid Mech.* **378**, 71–96.

Pirozzoli, S. 2010 Generalized conservative approximations of split convective derivative operators. *Journal of Computational Physics* **229**, 7180–7190.

Shahab, M. F., Lehnasch, G., Gatski, T. B. & Comte, P. 2011 Statistical characteristics of an isothermal, supersonic developing boundary layer flow from dns data. *Flow, turbulence and combustion* **86**, 369–397.

Shaupp, C., Sesterhenn, J. & Friedrich, R. 2008 On a method for direct numerical simulation of shear layer/compression wave interaction for aeroacoustic investigations. *Computers & Fluids* **37**, 463–474.

Shu, C.W. & Osher, S. 1988 Efficient implementation of essentially non-oscillatory shoch-capturing schemes. *Journal of Computational Physics* **77**, 439–471.

Suzuki, T. & Lele, S. 2003 Shock leakage through an unsteady vortex-laden mixing layer : application to jet screech. *J. Fluid Mech.* **490**, 139–167.

Ta'asan, S. & Nark, D.M. 1995 An absorbing buffer zone technique for acoustic wave propagation. In *AIAA Paper 95-0146*.

Tam, C. K. W. 1995 Supersonic jet noise. *Ann. Rev. Fluid Mech.* **27**, 17–453.

Thompson, K.W. 1987 Time dependent boundary conditions for hyperbolic systems. *J. Comp. Physics* **68**, 1–24.